Energy Conversion and Management 357 (2026) 121447

Contents lists available at ScienceDirect

Energy Conversion and Management

journal homepage: www.elsevier.com/locate/enconman

Thermal performance study of a TES system coupling solid–liquid and vapor–liquid phase change

Chaofan Qu [a], Zhaoxu Zhu [a], Yiming Xie [a], Xianbing Ji [a,b,*], Jinliang Xu [a,b], Zheng Miao [a,b]

[a] School of Energy Power and Mechanical Engineering, North China Electric Power University, Beijing 102206, China
[b] Beijing Key Laboratory of Multiphase Flow and Heat Transfer for Low Grade Energy Utilization, North China Electric Power University, Beijing 102206, China

ARTICLE INFO

Keywords:
Solid–liquid/vapor–liquid phase change coupling
Thermal energy storage
Thermal storage material
Erythritol

ABSTRACT

To address the limited heat transfer efficiency inherent in single phase change material (PCM) thermal energy storage (TES) systems, a TES method coupling solid–liquid and vapor–liquid phase changes was proposed, and a corresponding experimental system was established. By leveraging the near-isothermal characteristic and superior effective heat transfer coefficient of vapor–liquid phase change, the proposed approach overcame the limitations of conventional single phase TES systems, significantly enhancing both heat transfer performance and thermal efficiency. A series of experiments was conducted using erythritol as the solid–liquid phase change material and deionized water as the vapor–liquid phase change material to investigate the thermal performance of the system. The results indicate that the duration of heat storage and release increased with higher PCM filling ratios. The system sustained the production of vapor–water mixtures at temperatures exceeding 90.0 °C for 77.9 min, achieving an average heat release power of 6.68 kW. The addition of PCM increased the total heat release by 123.5% compared to the water-only condition and significantly prolonged the heat release duration. Furthermore, the system thermal efficiency improved with increasing PCM filling ratio, while the rate of gain gradually diminished. At a PCM filling ratio of 92.8%, the system achieved a thermal efficiency of 0.84. These findings provide valuable theoretical insights and practical guidance for the design and application of high efficiency thermal energy storage systems.

1. Introduction

As the global energy sector transitions toward a low-carbon mix, the integration of renewable energy and improved flexibility of coal-fired power plants have become key research priorities in energy storage research. Thermal energy storage technology plays a central role in mitigating the intermittency of renewables and enhancing overall energy efficiency, while also enabling industrial waste heat recovery and grid peak shaving support [1]. Among available options, phase change thermal storage stands out due to its high energy density and near-constant temperature discharge [2]. In summary, the performance of thermal storage systems is subject to inherent limitations of either solid–liquid or vapor–liquid PCMs when employed individually. Phase change thermal storage systems fall into two main types based on the physical state of the storage medium. One type is solid–liquid phase change storage, which uses materials such as molten salts and erythritol. The other type is vapor–liquid phase change storage, which relies on fluids such as water or organic compounds. Solid–liquid PCMs exhibit high latent heat capacity but suffer from low thermal conductivity, which limits their thermal charge/discharge rates. They are also prone to phase separation and supercooling [3]. In contrast, vapor–liquid PCMs enable rapid heat transfer via fast vaporization. However, their use in enclosed systems involves significant challenges: sharp pressure fluctuations during phase transition may raise safety issues, and the efficiency of latent heat utilization is limited by vapor diffusion kinetics [4]. The analysis clearly indicates that neither type of PCM alone can deliver fully efficient thermal storage.

To address these challenges, researchers have initiated innovative explorations of thermal storage materials. Hybrid phase change materials or systems incorporating synergistic solid–liquid and vapor–liquid phase change mechanisms enable such systems to combine high energy density with precise temperature control and enhanced heat transfer efficiency. This direction has garnered considerable attention from both academic and industrial communities. In the domain of hybrid phase-change materials research, the introduction of additives into PCMs has been demonstrated to significantly enhance thermal conductivity, thereby improving heat transfer efficiency. Carbon-based materials, metal oxides, and nanomaterials have all demonstrated considerable potential as effective PCM additives. Paul et al. [5] showed that while

* Corresponding author.

https://doi.org/10.1016/j.enconman.2026.121447
Received 26 January 2026; Received in revised form 22 March 2026; Accepted 2 April 2026
Available online 8 April 2026

Nomenclature

Q	heat, kJ/h
A	area, m^2
T	temperature, °C
p	pressure, Pa
V	volume, m^3
P	input power of the electric heating tubes, kW
m	flow rate, kg/h
c	specific heat capacity, kJ/(kg·K)
W	energy consumption, kW·h
H	enthalpy, J
g	acceleration due to gravity, m/s^2
Pr	Prandtl number
R	gas constant
C	coefficient
L	latent heat

Greek letters

η	thermal efficiency
ρ	density, kg/m^3
σ	surface tension, N/m
μ	dynamic viscosity
τ	transmittance

Abbreviations

HTF	heat transfer fluid
PCM	phase change material

Subscripts

HTF	for heat transfer fluid
PCM	for phase change material
sys	system
sat	saturated state
elec	electric heating tube
storage	for heat storage process
hr	for heat release process
l	liquid
p	constant pressure state

nanomaterial additives improve thermal conductivity in organic nanocomposite PCMs by reducing interfacial resistance, larger particles and higher concentrations cause agglomeration that reduces efficiency. But this effect necessitates careful control of additive concentration. Zhang et al. [6] reported that carbon nanomaterials like graphene and CNTs can boost PCM thermal conductivity by 137% while also enhancing cycling stability. These studies reveal that advancing composite PCMs depends not merely on conductive additives, but on a balanced design of composition, structure, and processing for target applications [7]. From the perspective of solid–liquid and vapor–liquid synergy, Hu et al. [8] developed a medium-temperature thermal storage unit that uses shaped PCM granules to integrate solid–liquid and vapor–liquid phase changes. It was experimentally demonstrated that this design mitigates performance limitation imposed by low PCM conductivity, limiting temperature difference between PCM and heat transfer fluid to 2 °C. Analysis indicates that synergistic coupling of high latent heat of solid-phase materials and rapid heat transfer characteristics of vapor–liquid phase change materials can simultaneously enhance both heat transfer efficiency and operational stability of the system. However, conventional selection criteria for working fluids, which depend on properties of single PCM, are no longer adequate [9]. Future efforts should focus on optimizing these criteria to meet multi-faceted requirements of hybrid systems, particularly in thermal synergy, interfacial compatibility, and dynamic stability between two types of phase change materials.

Thermal storage unit configuration critically influences heat storage/release performance. Researchers have proposed three primary configurations: direct-contact, indirect-contact, and heat-pipe-assisted systems. Subsequent research has examined thermal characteristics of these designs. The fundamental principle of direct-contact thermal storage entails integrating HTF and PCM within the same space to enhance heat transfer efficiency through direct contact. He et al. [10] constructed a direct-contact thermal storage device using erythritol as PCM and high-temperature thermal oil as HTF, conducting thermal performance experiments and simulations. Their study revealed that PCM melting process can be subdivided into three stages: channel stage, melting stage, and final stage. The incorporation of fins has been demonstrated to enhance the system's thermal storage efficiency by a factor of 270%. Subsequently, the team further optimized device structure by implementing a double-tube design at inlet and outlet of the direct-contact thermal storage unit [11]. Experimental results demonstrated that direct-contact configuration achieved superior thermal charging/discharging rates and required only a quarter of the thermal discharge time compared to indirect-contact systems. However, a significant drawback of direct-contact thermal storage is PCM's tendency to solidify and agglomerate, which can block HTF channels and reduce melting rate in subsequent cycles. To address this issue, Thon et al. [12] enhanced separation efficiency of a mixed solution of deionized water and methyl palmitate by adding surfactants. Their experiments demonstrated that the coalescence rate of the mixed solution exhibited approximately twofold enhancement compared to a reference system without surfactants. The indirect-contact thermal storage physically separates HTF and PCM within distinct chambers. This configuration offers greater flexibility in both working fluid selection and structural design, contributing to its broader applicability and relatively higher technological maturity. Kang et al. [13] investigated the influence of tube bundle and fin arrangements on thermal performance of an indirect-contact storage unit. Their results indicated that an optimized layout improved charging efficiency by 12.6% compared to a conventional uniform arrangement, while using Y-shaped fins enhanced storage efficiency by approximately 8.3% relative to straight fins. Al-Mudhafar et al. [14] enhanced thermal performance of a latent heat storage system by modifying a belly-tube heat exchanger. Experimental data showed this design reduced total solidification time of PCM by about 41% compared to systems using triple-tube or finned-tube heat exchangers. Additionally, Zhao [15] proposed a triple-tube spirally coiled thermal storage device. By utilizing centrifugal and torsional forces induced by fluid flow within the spiral coil, which promote secondary flow, the system thermal storage performance was further improved. Heat-pipe-assisted thermal storage integrates heat pipes—highly efficient heat transfer components—into the system to enhance charging and discharging efficiency. Maldonado et al. [16] compared thermal performance of shell-and-tube and heat-pipe assisted thermal storage systems, experimentally confirming that heat pipes effectively mitigate thermal shock within equipment, increasing system heat transfer rate by up to 40% under optimal conditions. Saraswat et al. [17] designed a semi-cylindrical container with heat pipes arranged perpendicular to axial direction, reducing PCM melting time from 12 h to 5.5 h. Zhao et al. [18] developed a novel embedded heat pipe for thermal storage applications. The system demonstrated exceptional temperature uniformity during PCM melting and solidification, with maximum axial and radial temperature differences of less than 5 °C and 12 °C, respectively. The constructed thermal energy storage module demonstrated capability to simultaneously store heat and provide heating.

Research on heat transfer enhancement in thermal energy storage

devices must consider piping as the core component for working fluid transport. Such research should focus on clarifying the heat transfer characteristics of different pipe configurations and optimizing their structures, particularly through cross-sectional shape optimization and internal fin structure improvement. In cross-sectional shape optimization, Saffarian et al. [19] compared circular and elliptical tubes under equal perimeter conditions using a water–air mixture as working fluid. Their findings showed that at a Reynolds number of 7000, the circular tube achieved an overall heat transfer coefficient of 8.9 W/(m^2·K), exceeding the elliptical tube's 6.9 W/(m^2·K), while also reducing pressure drop by 25%. Building on this, Mahato et al. [20] investigated twisted tubes with various cross-sectional geometries and found that, at a Reynolds number of 10,000 and a twist ratio of 16.5, the twisted square tube achieved a Nusselt number of 30—higher than that of the twisted hexagonal tube (Nu = 25). They also observed that although lower twist ratios increase the Nusselt number and enhance heat transfer, they simultaneously lead to higher flow resistance. Regarding external heat transfer characteristics, Kurşun et al. [21] studied heat transfer performance of circular, square, and triangular tubes using constant volume of n-eicosane as PCM. The results indicated that after 30.0 min of heating, the triangular tube demonstrated superior heat transfer performance compared to square and circular tubes, attributed to strong local natural convection generated at its corners. In regard to internal fin structure enhancement, Yu et al. [22] proposed novel bionic okra-shaped fins for thermal storage systems. Experiments confirmed that compared with straight fins, the okra-shaped fins increased melting rate by 58.46% and storage efficiency by 131.35%. When combined with Y-shaped topological fins, an additional 22.84% improvement in thermal performance was achieved. Tang et al. [23] developed a thermal storage system with discontinuous fins, achieving 23.4% reduction in PCM melting time and 36.7% improvement in temperature uniformity during charging versus conventional continuous fins. Zhang et al. [24] employed density-based topology optimization method to develop novel fin structures, which reduced PCM melting time by 35.2% and solidification time by 69.7% compared to conventional fins.

Furthermore, multi-stage PCM cascade systems significantly enhance thermal storage capacity by coupling multiple PCMs. This technique involves arranging different PCMs in a specific sequence and configuration to establish a cascade system that utilizes their distinct phase transition temperatures, thereby enabling the progressive storage of heat along the temperature gradient. For instance, Peiró et al. [25] conducted pilot-scale experiments on a multiple PCM cascade system, demonstrating that a dual PCM configuration improved average efficiency by 19.36% compared to a single PCM system. Similarly, Suyitno et al. [26] reported that a triple-PCM cascade increased average thermal charging power by 18.2% and thermal discharge efficiency by 29.5% compared to a single-PCM unit. Optimizing PCM arrangements and system geometry requires comprehensive investigation of factors influencing thermal performance in such systems. Rudra et al. [27] compared cylindrical and conical shell-and-tube heat exchangers, demonstrating that the conical design more effectively utilizes natural convection to enhance heat transfer, achieving 17.6% higher average discharge power. In a study on PCM arrangement, Elsanusi et al. [28] found that series and parallel configurations reduced PCM melting time by approximately 15.5% and 9.3%, respectively, compared to a single-PCM layout. This discrepancy was attributed to the interplay between conduction and convection: parallel arrangements enhance heat conduction while simultaneously suppressing natural convection.

Analysis of the above literature indicates that despite significant research and progress in the field of multiphase thermal energy storage, exploratory applications of thermal storage systems integrating coupled solid–liquid and vapor–liquid phase changes remain relatively scarce. Further investigation is needed into the thermal performance and synergistic mechanisms of such coupled systems under practical operating conditions. To address this limitation, this study proposes a TES system that couples solid–liquid phase change and vapor–liquid phase change to enhance the overall thermal performance of the TES system. Using erythritol (solid–liquid phase change material) as PCM and water (vapor–liquid phase change material) as HTF, a hybrid experimental TES system was constructed. The study systematically investigated the thermal performance characteristics during heat storage and release, the melting and solidification mechanisms of the PCM, and the thermal efficiency throughout complete heat storage/release cycles. The technology shows potential for application in scenarios such as short-term, cross-time-scale thermal energy storage, efficient recovery of industrial waste heat, and coordinated thermal-electric control in multi-energy complementary systems.

2. Construction of TES system coupling solid–liquid and vapor–liquid phase change

2.1. System construction

The experimental TES system that couples solid–liquid and vapor–liquid phase changes is shown in Fig. 1. The system primarily consists of a thermal storage device, a cooling water tank, and control/data acquisition equipment. The thermal storage device contains four main components. The heat source comprises two electric heating tubes installed at the bottom of the device, providing a continuous and stable heat input of 35.0 kW to the system. The PCM section consists of the PCM and its encapsulated tube shell with internal fins. The PCM is encapsulated within these tubes, which are collectively mounted on a perforated partition above the heat source. This perforated partition facilitates the flow of HTF between the heat source and the PCM section, enabling heat transfer. The HTF section features a vapor–liquid phase change material that fills the gap between the thermal storage tank and the PCM tubes, serving as the medium for heat transfer between various system components. The condensation section primarily consists of the heat exchanger coil at the top of the device, external circulation piping, and associated power equipment. The cooling water tank, along with its associated piping and pump, provides the coolant for the thermal storage device. Auxiliary components for the thermal storage system include saddles, piping, and related accessories.

The thermal storage device must withstand temperatures exceeding the phase change temperature of the PCM and pressures exceeding the vapor pressure of the HTF at the corresponding temperature. The key design parameters provided in Table 1 include a design pressure of 0.90 MPa, a design temperature of 180.0 °C, and internal dimensions of 1400.0 mm × Ø700.0 mm. To address the low thermal conductivity of polyol-based PCMs (e.g., erythritol) and the consequent difficulty in melting their central regions—which often leads to prolonged heat storage times—three radial fins were incorporated inside the PCM encapsulation tubes. The geometric and material parameters of these fins are listed in Table 2. These fins were made of aluminum alloy with dimensions of 1350.0 mm × Ø50.0 mm × 0.5 mm, and leverage the metal's superior thermal conductivity to transfer heat from multiple directions to the central region of the PCM, thereby effectively accelerating the melting process at the center of the PCM, enhancing the system's heat storage efficiency [29].

2.2. Heat storage/release process

To elucidate the thermal storage process that couples solid–liquid and vapor–liquid phase changes, the internal structure of the thermal storage device is depicted in Fig. 2. During the heat storage mode, heat generated by the electric heating tubes is absorbed by the HTF. Once heated to its boiling point, the HTF vaporizes. The resulting vapor condenses on the outer wall of the PCM tubes, releasing latent heat. The heat is then conducted through the shell and internal fins to the PCM inside the tube, raising its temperature to the phase change point (117.0 °C) and initiating melting. The heat storage process concludes when the phase change material is fully melted. When the system switches to heat

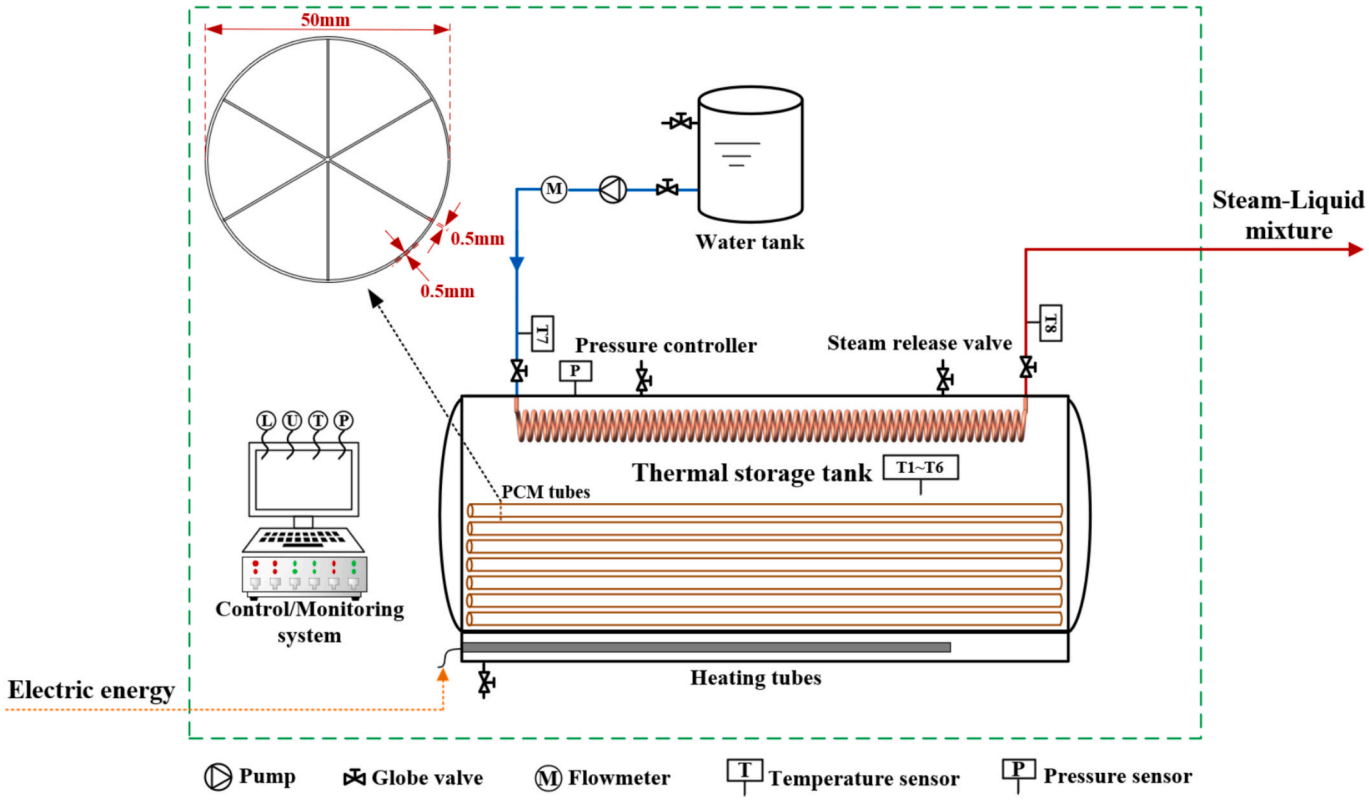

Fig. 1. TES system coupling solid–liquid and vapor–liquid phase change.

Table 1
Parameters of thermal energy storage system.

Parameters	Values	Unit
Main material	stainless steel	–
Design pressure	0.90	MPa
Design temperature	180.0	°C
Volume	0.63	m^3
Inner cylinder diameter	700.0	mm
Inner cylinder length	1400.0	mm

Table 2
Parameters of PCM tube.

Parameters	Values	Unit
Main material	aluminum alloy	–
Length	1350.0	mm
Inner diameter × outer diameter	49.0 × 50.0	mm
Fin length	1350.0	mm
Fin thickness	0.5	mm
Filling PCM quality	1.92	kg

release mode, the circulation pump in the condensation system starts up, circulating cooling water through the heat exchange coil. At this point, the gaseous heat transfer fluid condenses and liquefies on the outer surface of the coil, transferring heat to the cooling medium. The liquefied HTF drips back into the liquid pool, where it absorbs heat released during the solidification of the PCM and re-vaporizes, rising again to the coil's outer surface to condense. This forms a continuous cycle of HTF vaporization and condensation, enabling sustained heat release until the temperature of the medium at the coil outlet no longer meets the operational requirements.

The system achieves efficient heat transfer through the synergistic interaction of four components within the thermal storage device, with its configuration adapted to the operating mode. During heat storage mode, the heat source, HTF, and PCM module form a heat pipe–like configuration. HTF absorbs heat and vaporizes at the heat source, then condenses and releases heat at the PCM tubes. This phase change cycle is coupled with the PCM's melting process. By utilizing HTF's high effective heat transfer capacity and near-isothermal phase change behavior, efficient heat storage in the PCM is achieved. During heat release mode, a similar heat pipe–like configuration is established among the PCM, HTF, and condenser module. HTF vaporizes by absorbing heat from the PCM and condenses to release heat at the coil. This phase change cycle is coupled with the PCM's solidification process, enabling continuous and efficient heat release.

The thermodynamic principle of solid–liquid and vapor–liquid coupled thermal storage is the vapor–liquid phase equilibrium of the HTF. Through the synergistic variation of temperature and pressure, the thermal storage and release cycle is sustained. This mechanism is quantitatively described by the Clausius–Clapeyron equation:

$$\frac{dp}{dT} = \frac{\Delta H_{HTF}}{T(V_g - V_l)} \tag{1}$$

$$\ln\left(\frac{P_2}{P_1}\right) = -\frac{\Delta H_{HTF}}{R}\left(\frac{1}{T_2} - \frac{1}{T_1}\right) \tag{2}$$

where p is the system pressure, Pa; T is the temperature of the TES, K; ΔH_{HTF} is the phase change enthalpy of the HTF, J/kg, V_g is the molar volume of water vapor, m^3/mol, V_l is the molar volume of water, m^3/mol; P_1, P_2 are the saturation pressures corresponding to saturation temperatures T_1, T_2, Pa; R is the gas constant for water vapor, 461.5 J/(kg·K).

Based on the positive correlation between the saturated temperature and pressure of the HTF described by Equations (1) and (2), the system maintains a dynamic equilibrium throughout the heat storage and release processes. During the heat storage process, continuous HTF vaporization causes simultaneous increases in the internal saturated pressure and saturated temperature of the device. This equilibrium

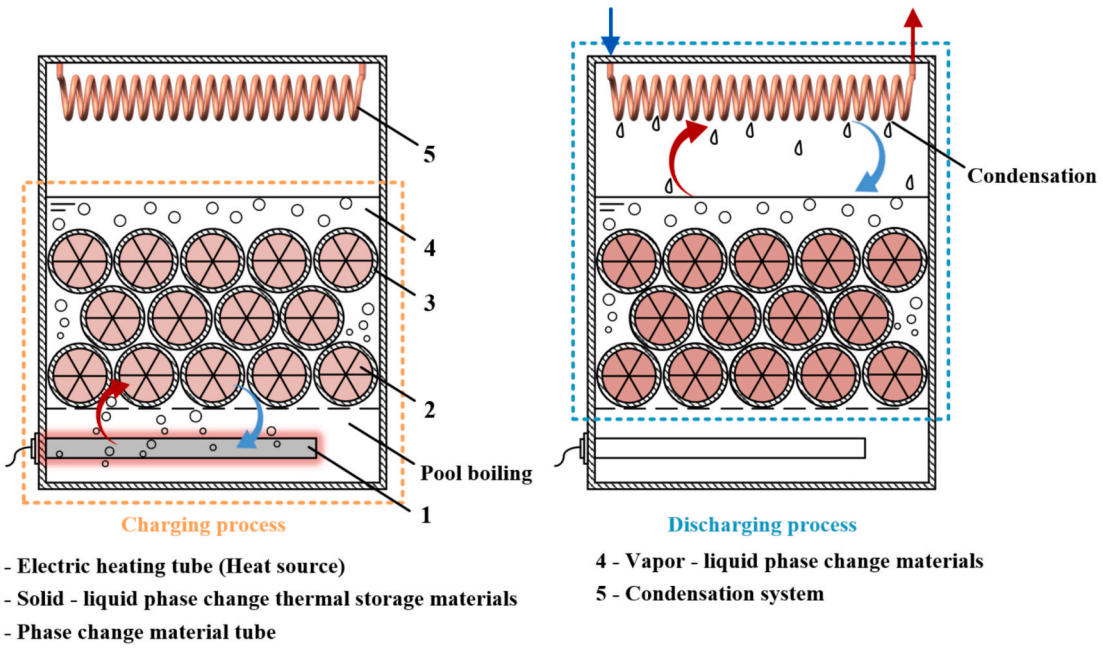

Fig. 2. Schematic of the heat exchange structure combination for the TES system coupling solid–liquid and vapor–liquid phase change.

ensures the HTF's vapor–liquid cycle and sustained heat transfer to the PCM. During the heat release process, coolant flowing through the coil induces HTF condensation, causing the internal pressure to drop. Notably, this process does not involve true superheating of the liquid. The sudden pressure drop causes the high-temperature liquid—now above its saturation temperature at the new pressure—to undergo rapid phase change. This mechanism allows the HTF to continuously transition between equilibrium states within a defined temperature and pressure range that fully encompasses the PCM's solidification interval. The PCM exhibits negligible volume variation during solidification, and its melting point is pressure-independent. The heat released during solidification is utilized to sustain the HTF's superheated state and subsequent flash vaporization.

The intensity of flash vaporization is primarily determined by the superheat—the difference between the liquid temperature and the saturation temperature at the reduced pressure—induced by a pressure drop. During early heat release, the high system temperature yields large apparent superheat, causing intense flash vaporization. As the process continues, the temperature drops, reducing apparent superheat and weakening flash vaporization. Phase change occurs via bulk flash vaporization, not surface boiling. The relationship between apparent superheat and heat flux density can be expressed as:

$$q = \mu_l \Delta H_{vap} \sqrt{\frac{g(\rho_l - \rho_{vap})}{\sigma}} \left(\frac{c_{p,l}(T_l - T_{sat})}{C_{s,f} \Delta H_{HTF} Pr_l^n} \right)^3 \quad (3)$$

where q, is the heat flux density, W/m^2; μ_l is the dynamic viscosity of the liquid HTF, Pa·s; g is the gravitational acceleration, m/s^2, ρ_l is the density of the liquid HTF., kg/m^3, ρ_{vap} is the density of the gaseous HTF, kg/m^3; σ is the surface tension of the HTF, N/m; $c_{p,l}$ is the isobaric specific heat capacity of the liquid HTF, J/(kg·K); T_l is the temperature of the liquid condensed HTF, K; T_{sat} is the saturation temperature at the current pressure, K; $C_{s,f}$, n are the empirical constant; Pr_l is the Prandtl number of the liquid HTF.

Compared to single solid–liquid phase change or vapor–liquid phase change thermal storage systems, the system that couples solid–liquid and vapor–liquid phase changes developed in this study demonstrates significant advantages in both its dynamically integrated heat transfer structure and the synergistic interactions. Single solid–liquid phase change thermal storage systems commonly exhibit thermal lag due to low material thermal conductivity, where the outer layer melts while the interior remains solid. Integrating a water vapor cycle into the solid–liquid phase change heat storage/release cycle establishes a heat pipe–like efficient heat transfer pathway between the PCM and the heat source/condensation system, effectively mitigating this issue. Additionally, solid–liquid PCM systems exhibit high volumetric heat storage density. For example, erythritol provides a high volumetric heat storage density (200–300 kJ/L), enabling more compact thermal storage systems. However, they are limited by slow heat transfer. In contrast, vapor–liquid phase change systems exhibit rapid heat transfer—for instance, water vapor condensation achieves significantly higher heat transfer coefficients than conduction in erythritol—but possess lower energy storage density. The synergistic integration of both systems provides complementary physical properties. In summary, this system achieves a synergistic enhancement of thermal storage capacity, heat transfer rate, and exergy efficiency through the dual coupling of structure and material properties.

2.3. Material selection

In theory, any substance capable of undergoing phase transitions such as solid–liquid, liquid–vapor, solid–vapor, or solid–solid can be classified as a PCM. Among these, solid–liquid PCMs are the most widely used in thermal energy storage, owing to several favorable properties: minimal volume change during phase transition, a broad phase transition temperature range, excellent thermal cycling stability, tunable thermal conductivity, chemical stability, and corrosion resistance [3]. In contrast, working fluids that undergo vapor–liquid phase change (e.g., water) possess higher latent heat of vaporization and exhibit a significant decrease in density after phase transition, resulting in a large expansion of vapor volume. Designing the system as a pressure vessel can mitigate the issue of bulky equipment; however, it introduces safety risks associated with the high-pressure steam generated during operation. To comprehensively investigate a material's energy storage capacity, volumetric energy density is commonly used—defined as the amount of energy stored per unit volume of the storage medium. Its calculation formula is as follows:

$$E_v = L \times \rho \quad (4)$$

where E_v is the volumetric energy density, J/m^3; L is the latent heat value of the medium, J/kg; ρ is the density of the phase change material in its energy storage state, kg/m^3. Preliminary calculations indicate that erythritol exhibits a significantly higher volumetric energy density than water. When storing the same amount of energy, erythritol has a volumetric energy density 364 times greater than water and approximately 42 times greater than water at 10 atmospheres of pressure.

The selection of solid–liquid phase change materials for the constructed thermal storage system must fulfill two core requirements. First, the phase change temperature range of the solid–liquid phase change material must overlap with the operating temperature range of the vapor–liquid phase change material to ensure synergistic operation. Second, the material must exhibit excellent compatibility with the thermal storage device container. Based on these criteria, erythritol was selected in this study as the solid–liquid phase change thermal storage material. Erythritol is a tetrahydric sugar alcohol with a molecular weight of 122.12 g/mol. As a promising medium to low temperature PCM, it exists as a white crystalline powder at room temperature and is odorless. As shown in Table 3, this material has a phase change temperature range of 117.0–120.0 °C, with a latent heat of approximately 334.0 kJ/kg, making it ideally suited for medium to low temperature thermal energy storage applications.

The selection of a vapor–liquid phase change material must satisfy three criteria. Its phase change temperature range must cover that of the solid–liquid PCM, the internal pressure within the device after vaporization must remain within safe operational limits, and long-term chemical and physical compatibility with the container material must be ensured. The saturation temperature of water increases systematically with pressure and fully encompasses erythritol's phase change temperature range (117.0–120.0 °C) at pressures well below typical safety thresholds for pressure vessels. Therefore, water was selected as the vapor–liquid phase change material.

3. Test methods and error analysis

3.1. Test methods

Fig. 3 illustrates the experimental setup of the solid–liquid coupled vapor–liquid phase change thermal energy storage system. The temperature monitoring system consists of nine sensors positioned to monitor temperatures at critical locations. Class A three-wire PT100 RTDs are utilized to measure the HTF temperature (T1–T5), the coolant inlet and outlet temperature (T7–T8), and the ambient temperature (T9). The PCM temperature (T6) is measured using a Class 1 precision Type K armored thermocouple. Inserted directly into the central PCM tube, this sensor serves as a conservative indicator to determine the completion of the phase transition. Furthermore, the penetration point of the PCM tube is sealed with high-temperature-resistant sealant to prevent leaks. The coolant flow rate is actively regulated by a micro-gear pump equipped with an integrated flow sensor. A YD-305 pressure transmitter is used to monitor the internal pressure of the thermal storage device. Electrical heating power is supplied directly from the control cabinet. Table 4 summarizes the specifications of the test equipment used in the experimental setup. All sensor signals were acquired and recorded using an Agilent 34970A data acquisition unit.

Table 3
Parameters of the PCM.

Properties	Value	Unit
Phase change temperature	117.0 – 120.0	°C
Latent heat capacity	334.0	kJ/kg
Thermal conductivity	0.25(solid)/0.20(liquid)	W/(m·K)
Specific heat	1.45(solid)/2.40(liquid)	kJ/(kg·K)
Density	1470.00(solid)/1250.00(liquid)	kg/m^3
Viscosity	0.01 – 0.05	kg/(m·s)

Before each experiment, all test conditions strictly adhere to standardized preparation procedures to ensure consistency and reproducibility of initial states. First, the required quantity of PCM tubes is loaded into designated positions according to target operating conditions. Subsequently, the piping and internal components are flushed with deionized water at room temperature to remove potential residual contaminants. After flushing, the sealing door is closed, and deionized water is injected through the HTF inlet until the PCM tubes are fully submerged. Upon completion of preparations, the system is activated via the control cabinet and immediately operates according to the preset control logic.

The control logic of the thermal storage system is illustrated in Fig. 4. Considering the energy transfer characteristics of the coupled solid–liquid and vapor–liquid phase change system and user heat demand, three operational modes are defined: heat storage, heat preservation, and heat release. The automatic control system acquires real-time data via temperature and pressure sensors, coordinating with actuators, including electric heaters and circulation pumps, to transition between operational modes based on preset logic.

Upon initiating heat storage mode, electric heaters convert electrical energy into thermal energy, which is absorbed by the HTF within the thermal storage device. The HTF is heated until it reaches its boiling point and vaporizes. The generated vapor condenses on the outer surface of the PCM tube, releasing latent heat that transfers to the PCM and causes its temperature to rise continuously. Once the PCM temperature exceeds the phase change plateau and continues to increase, eventually reaching 130.0 °C, the system completes the heat storage process and transitions to heat preservation mode. Thermal losses are primarily minimized by the external insulation layer, with low-power heating providing auxiliary support to maintain stable internal temperature. When heat is demanded, the system switches to heat release mode. The circulation pump activates, driving the coolant through the heat exchange coils. HTF vapor condenses on the coil surfaces, releasing heat to the coolant. Depending on the coolant flow rate and inlet conditions, the system delivers hot water, steam–water mixtures, or saturated steam. When the outlet temperature drops below the setpoint, the circulation pump deactivates, terminating the heat release process.

To systematically investigate the heat storage and release performance of the TES system, experiments were executed following the aforementioned control strategy. Three operating conditions were established by varying the PCM loading quantity: systems configured with 20, 40, and 60 PCM tubes (utilizing water as the HTF). A corresponding water-only thermal storage system served as the control group. All test conditions initiated under identical initial conditions (system equilibrated at ambient temperature) to ensure comparability. Each condition underwent three repeated heat storage/discharge cycles starting from the initial state. During heat release, the liquid fraction of the steam-water mixture at the heat exchanger outlet was monitored at 10.0 min intervals to facilitate analysis of heat release power trends across conditions. Average heat release power was calculated using inlet and outlet temperatures and the coolant mass flow rate. To investigate system thermal efficiency, experimental series were conducted with incrementally increasing PCM filling ratios, each comprising three consecutive cycles. Thermal efficiency was defined as the ratio of net heat output to total energy input during continuous system operation.

During the heat storage process, a portion of the electrical energy input to the system is converted into the sensible and latent heat of the PCM and HTF, while another portion is the heat loss of the device. Based on this energy conversion principle, the overall energy balance can be expressed as:

$$\int_0^t P_{elec} dt = Q_{HTF} + Q_{PCM} + Q_{loss} \tag{5}$$

where P_{elec} is the power of the heating rods, kW; Q_{HTF} is the heat absorbed by the HTF, kW·h; Q_{PCM} is the heat absorbed by the PCM,

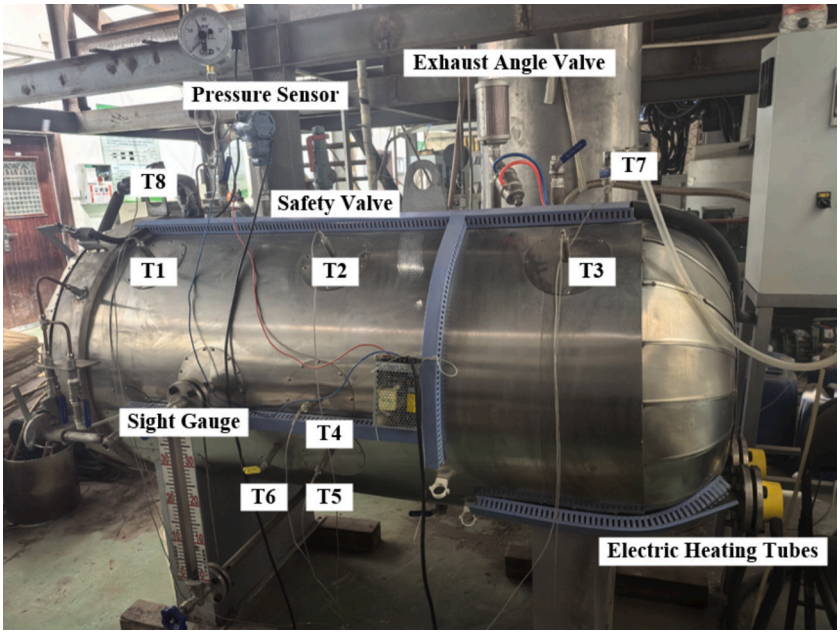

Fig. 3. Experimental setup of the TES system coupling solid–liquid and vapor–liquid phase change.

Table 4
Specifications of the test equipment.

Equipment	Specifications	Manufacturer
PT100 RTD	Temperature Range: −200.0–450.0 °C, Accuracy Class A, Resolution: 0.01℃	Wanyang Automation Equipment Co., Ltd.
K-type Armored Thermocouple	Temperature Range: 0.0–800.0 °C, Accuracy Class 1, Resolution: 0.01 °C	Omega Engineering, Inc.
WT3000-1FB Micro Gear Pump	Flow Range: 85.7–2571.4 ml/min, Resolution: 0.92 ml/min	Baoding Lange Constant Flow Pump Co., Ltd.
YD-305 pressure transmitter	Pressure Range: 0–0.7 MPa, Accuracy: 0.25%, Resolution: 0.07 kPa	Huai'an Yuanda Automation Instrument Co., Ltd.

kW·h; Q_{loss} is the heat loss of the thermal storage device, kW·h.

The heat absorbed by the HTF (Q_{HTF}) can be expressed as:

$$Q_{HTF} = m_{HTF}\left(h_f + xL_{HTF} - h_g\right) \tag{6}$$

where m_{HTF} is the HTF mass, kg; L_{HTF} is the latent heat of the HTF, kJ/kg; h_f is the specific enthalpy of saturated liquid, kJ/kg; h_g is the specific enthalpy of saturated vapor, kJ/kg; x is the vapor mass fraction, $0 \le x \le 1$.

The heat absorbed by the PCM (Q_{PCM}) can be calculated using a three-stage model based on its melting process:

$$Q_{PCM} = \begin{cases} m_{PCM}c_{p,solid}(T_{PCM} - T_0) & T_{PCM} < T_m \\ m_{PCM}\left[c_{p,solid}(T_m - T_0) + f_l L_{PCM}\right] & T_{PCM} = T_m \\ m_{PCM}\left[c_{p,solid}(T_m - T_0) + L_{PCM} + c_{p,liquid}(T_{PCM} - T_m)\right] & T_{PCM} > T_m \end{cases} \tag{7}$$

where m_{PCM} is the PCM mass, kg; L_{PCM} is the latent heat of the PCM, kJ/kg; T_0, T_m and T_{PCM} are the initial PCM temperature, PCM melting temperature, and current PCM temperature, respectively, K; $c_{p,solid}$ is the heat capacity of the PCM in the solid phase, kJ/(kg·K); $c_{p,liquid}$ is the heat capacity of the PCM in the liquid phase, kJ/(kg·K); f_l is the liquid fraction of the PCM, $0 \le f_l \le 1$. Only when the PCM is fully molten ($f_l = 1$) can its temperature rise above T_m. Therefore, the condition$T_{PCM} > T_m$is used to identify the completion of melting in this study.

Heat storage power is defined as the effective heat flux transferred to the PCM per unit time by the storage device, primarily used to characterize the system's heat storage rate. The equations for calculating the heat storage capacity ($Q_{storage}$) and heat storage power ($P_{storage}$) are given as follows [30]:

$$Q_{storage} = \int_{t1}^{t2} (Q_{PCM} + Q_{HTF})dt \tag{8}$$

$$P_{storage} = \frac{Q_{storage}}{\Delta\tau} \tag{9}$$

During the heat release process, the energy released by the PCM drives the flash vaporization–condensation cycle of the HTF, and the heat transfer can be described by the following equation:

$$P_{hr} = m_{PCM}L_{PCM}\frac{d\phi}{dt} + (mc_p)_{sys}\frac{dT_{sys}}{dt} + L_{HTF}\frac{dm_v}{dt} \tag{10}$$

where P_{hr} is the heat release power, kW; $d\phi$ is the liquid fraction of the PCM; $(mc_p)_{sys}$ is the total heat capacity of the system, kJ/K; T_{sys} is instantaneous average temperature of the system, K; m_v is the mass of water vapor, kg.

The heat release performance of the system can be quantified and characterized by two core indicators: heat release power (P_{hr}) and heat release capacity (Q_{hr}). These parameters are calculated as follows:

$$P_{hr} = c_{p,water}m_{water}\Delta T \tag{11}$$

$$Q_{hr} = \tau c_{p,water}m_{water}\Delta T \tag{12}$$

where m_{water} is the mass flow rate of the cooling water, kg/h; $c_{p,water}$ is the constant pressure specific heat capacity of water in the heat exchange coil, kJ/(kg·K); τ is the time, hour.

During the complete operational cycle of the thermal storage system, the thermal efficiency serves as the indicator for investigating the overall energy conversion and utilization level. The thermal efficiency serves as the primary metric for evaluating the overall energy conversion and utilization performance across the complete operational cycle. It is defined as the ratio of the effective heat output during the heat release process to the total energy input during the storage phase. This parameter reflects the cumulative thermal losses level incurred from input to output, providing a critical basis for assessing the system's

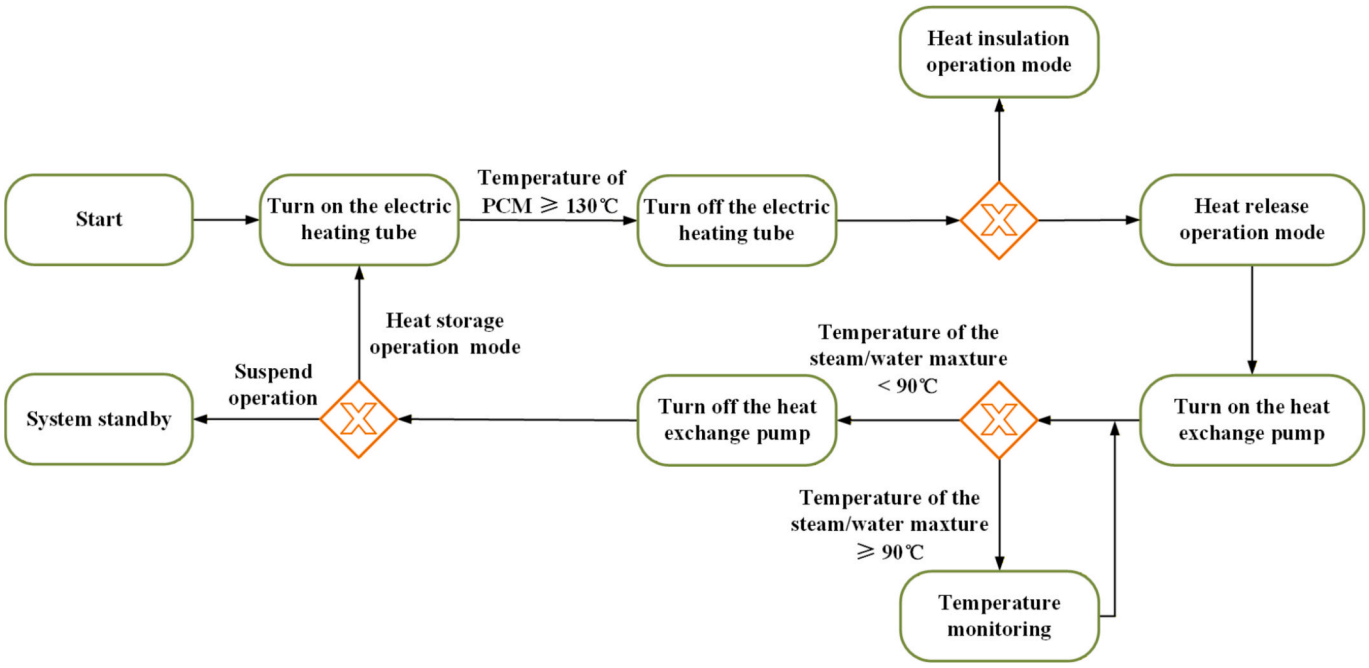

Fig. 4. Control logic of the TES system coupling solid–liquid and vapor–liquid phase change.

holistic performance. The thermal efficiency (η_{sys}) is calculated as follows:

$$\eta_{sys} = \frac{Q_{hr}}{Q_{ht}} \times 100\% \tag{13}$$

where Q_{ht} is the total energy input to the thermal storage device by the electric heating rods, kW·h.

3.2. Error analysis

In the present experiment, measurements of parameters such as temperature, flow rate, and power exhibit inherent uncertainties due to instrument limitations and environmental disturbances. Specifically, the relative uncertainties, accounting for both instrumental precision and experimental variability induced by multi-phase flow fluctuations, are quantified as 2.08% for the PT100 RTD, 1.92% for the K-type thermocouples, and 2.05% for the mass flow rate measurements. Consideration of the power regulator used in the power control of the electric heating elements results in an electrical power uncertainty of 1.89%. Performance parameters—including heat storage power, heat release power, and system thermal efficiency—require indirect calculation based on these direct measurements, causing errors to propagate through the computational process to the final results. The uncertainty calculation method based on error propagation theory is as follows:

$$y = f(x_1, x_2, x_3, \ldots, x_n) \tag{14}$$

$$\Delta y = \left[\left(\frac{dy}{dx_1} \Delta x_1 \right)^2 + \left(\frac{dy}{dx_2} \Delta x_2 \right)^2 + \left(\frac{dy}{dx_3} \Delta x_3 \right)^2 + \ldots + \left(\frac{dy}{dx_n} \Delta x_n \right)^2 \right]^{\frac{1}{2}} \tag{15}$$

where x_n is the independent variable, y is the experimental result, Δx_n is the measurement error of each instrument, Δy is the absolute error of the measured value. The system's heat release power (P_{hr}) and heat release capacity (Q_{hr}) are related to the coolant temperature (PT100 RTD) and flow rate. Their uncertainty can be expressed as:

$$\frac{\Delta P_{hr}}{P_{hr}} = \sqrt{\left(\frac{\Delta m_{water}}{m_{water}} \right)^2 + \left(\frac{\Delta T_{in}}{T_{out} - T_{in}} \right)^2 + \left(\frac{\Delta T_{out}}{T_{out} - T_{in}} \right)^2} \tag{16}$$

$$\frac{\Delta Q_{hr}}{Q_{hr}} = \sqrt{\left(\frac{\Delta m_{water}}{m_{water}} \right)^2 + \left(\frac{\Delta T_{in}}{T_{out} - T_{in}} \right)^2 + \left(\frac{\Delta T_{out}}{T_{out} - T_{in}} \right)^2} \tag{17}$$

Similarly, the system thermal efficiency(η_{sys}) is related to the coolant temperature (PT100 RTDs), flow rate, and electric heating power. Its uncertainty can be expressed as:

$$\frac{\Delta \eta_{sys}}{\eta_{sys}} = \sqrt{\left(\frac{\Delta m_{water}}{m_{water}} \right)^2 + \left(\frac{\Delta T_{in}}{T_{out} - T_{in}} \right)^2 + \left(\frac{\Delta T_{out}}{T_{out} - T_{in}} \right)^2 + \left(\frac{\Delta P_{elec}}{P_{elec}} \right)^2} \tag{18}$$

Calculations indicate that the combined uncertainty in the system's heat release power and capacity is 3.59%, while the uncertainty in thermal efficiency is determined to be 4.05%. The analysis confirms that all experimental deviations remain within theoretically acceptable limits, thereby validating the accuracy and reliability of the reported results.

4. Results and discussion

4.1. Heat storage performance

Fig. 5 illustrates the temperature variation trends within the thermal storage device during the heat storage process under conditions of the water-only and varying PCM tube loads (20, 40, and 60 tubes, corresponding to filling ratios of 14.3%, 28.6%, and 42.9%, respectively). Fig. 5(a) specifically shows the internal temperature variation trend under the water-only condition. It could be observed that the temperature trends at the top, middle, and bottom of the device were generally consistent. The HTF heating process could be divided into two stages: the heating stage and the temperature maintenance stage. When the heating tubes started up, the HTF temperature rose rapidly across all regions. After 8.6 min, temperatures in all regions reached 130.1 °C and stabilized, with the internal system pressure at approximately 0.35 MPa. Overall, during both the heating and temperature maintenance stages,

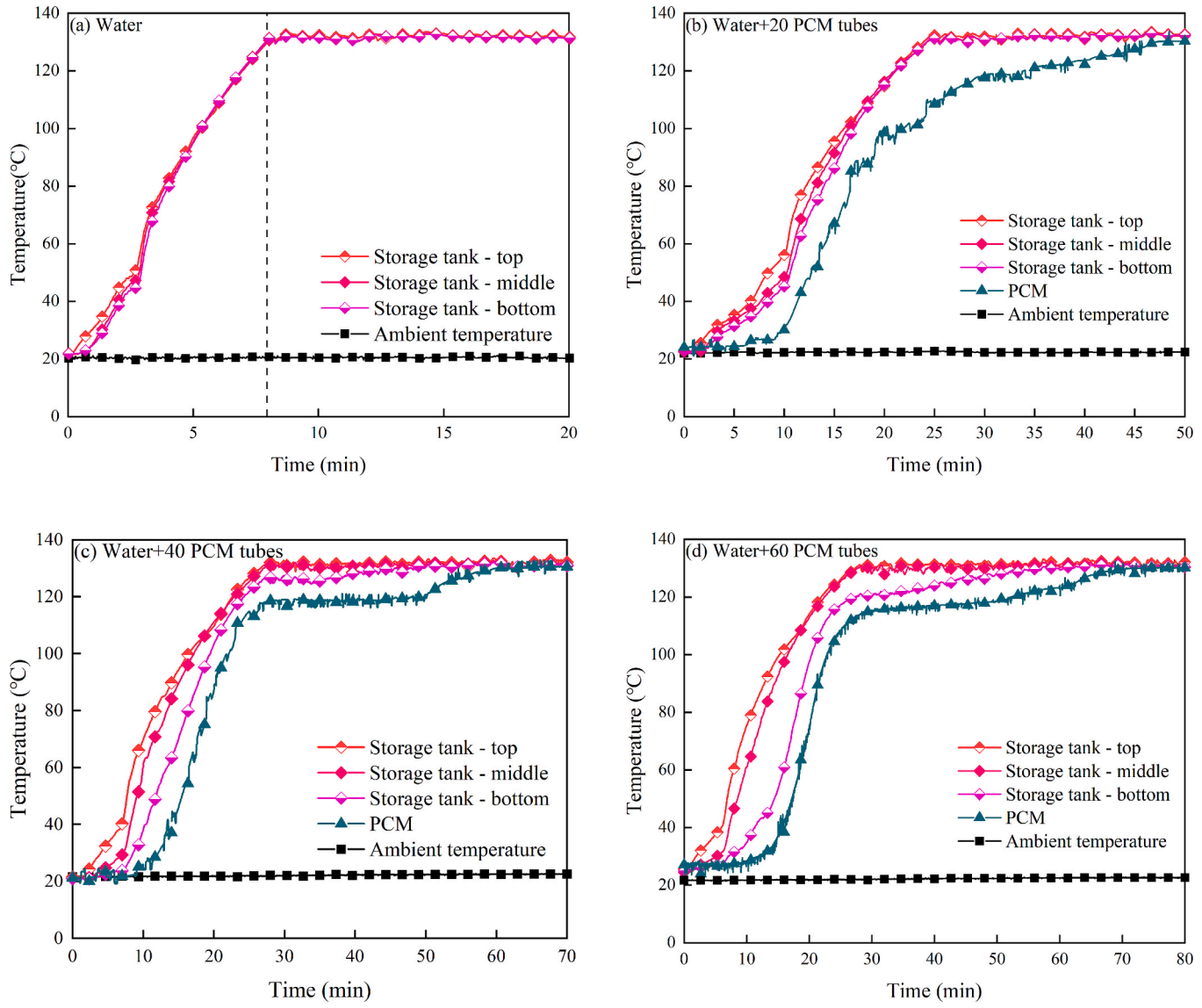

Fig. 5. Temperature during heat storage in the TES system coupling solid–liquid and vapor–liquid phase change.

the temperature differences between the top, middle, and bottom sections of the device were small, with a maximum temperature difference of 8.9 °C.

Fig. 5(b) presents the temperature variation trends within the thermal storage device during the heat storage process under the condition of 20 PCM tubes loading quantity. In initial state, the temperature distribution within the device was relatively uniform, with an average temperature of 22.7 °C across all regions including PCM. The heat storage process could be divided into three stages based on the phase change behavior of the PCM. ***Stage I (PCM sensible heating absorption and HTF latent heat absorption)***: HTF temperature increased from initial temperature of 22.4 °C to boiling point of 100.0 °C. Once HTF temperature significantly exceeded that of PCM, heat transfer rate increased and drove PCM temperature to rise gradually. Due to the thermal response characteristics of PCM, its temperature increase lagged behind that of HTF. As heating continued, the HTF reached a steady state at 130.0 °C and maintained a saturated vapor state, while the system pressure simultaneously rose to 0.35 MPa. Meanwhile, PCM continued to be heated, with its temperature approaching the phase change point of 117.0 °C. In this process, the HTF primarily absorbed heat as latent heat, while the PCM continued to store heat primarily as sensible heat. ***Stage II (PCM melting stage)***: When the PCM temperature reached its phase change point of approximately 117.0 °C, solid–liquid phase change began. In this stage, the HTF temperature and pressure remained stable, while the PCM temperature fluctuated between 116.9 °C and 118.5 °C until complete melting. This stage concluded when the PCM was fully melted, manifested by the PCM temperature transitioning from a plateau to a gradual rise. The form of heat absorption within the system changed. The heat absorbed by the HTF was primarily in the form of sensible heat, while the PCM primarily stored heat as latent heat. ***Stage III (PCM sensible heating stage)***: HTF temperature and system pressure remained stable, while the liquid PCM temperature continued to rise. Its temperature gradually increased to approximately 130.0 °C, eventually reaching thermal equilibrium. The heat absorbed by the PCM was entirely stored as sensible heat in this stage.

Fig. 5(c) and Fig. 5(d) illustrate the temperature variation trends within the thermal storage device during the heat storage process under 40 and 60 PCM tubes loading quantity conditions, respectively. Analysis indicated that the heat storage process under different PCM loading quantities followed the aforementioned three stage pattern, with consistent temperature variation trends across all regions of the device.

As the PCM tube load increased sequentially from 20 to 40 and then to 60, the total heat storage time extended from 46.3 min to 59.6 min and finally to 71.5 min. While temperature evolutions at the top and

middle sections remained largely synchronized, the bottom section exhibited a progressive thermal lag with increasing PCM mass. This delayed temperature rise resulted in a maximum vertical temperature gradient of 47.9 °C between the bottom and top regions. This phenomenon is primarily attributed to the increased total heat demand required to heat the larger PCM mass. Heat supplied by the bottom HTF was continuously absorbed by the PCM for sensible heating and melting, significantly retarding the temperature rise rate compared to the middle and top sections. Consequently, the thermal response disparity became more pronounced as the system's thermal inertia grew with the added PCM mass, thereby amplifying the vertical temperature gradient during charging. The PCM melting durations for the three loads were 8.1 min, 17.1 min, and 24.6 min, respectively. This further confirms that increasing the PCM loading quantity prolongs its melting duration, thereby extending the total heat storage time of the system.

Analysis shows that integrating PCM significantly enhances thermal storage capacity compared to a water-only system under identical volumetric constraints and final charging temperature. In the water-only system, energy is stored primarily as sensible heat, with an additional contribution from the latent heat associated with partial vaporization in the sealed environment; its total stored heat is calculated using Equation (6). In contrast, the PCM-integrated system stores thermal energy through three components: the sensible heat of water, the latent heat of water vaporization, and the heat absorbed by the PCM, with the total storage capacity given by Equation (7). Over the temperature range of 22.5 °C to 130.0 °C, the water + 20 PCM tubes condition achieves a total heat required of 16.21 kW·h—approximately 198.5% higher than the 5.43 kW·h achieved by the water-only system. This substantial increase demonstrates that PCM integration effectively enhances volumetric energy storage density within the same physical volume.

Fig. 6 illustrates the heat transfer mechanism within the thermal storage device and the PCM melting mechanism during the heat storage process. The heat transfer mechanism during the system's heat storage operation, as shown in Fig. 6(a), is fundamentally a vapor–liquid phase change heat transfer process driven by the heat stored within the PCM. Electric heating tubes continuously heat the HTF to its boiling point, inducing vigorous boiling and generating a multitude of vapor bubbles. These bubbles, acting as latent heat carriers, rise under buoyancy to impinge upon the cooler outer walls of the PCM tubes. Upon contact, the vapor rapidly releases its latent heat and condenses. This phase transition triggers a sharp internal pressure drop, causing the bubbles to implode under the surrounding liquid pressure. The released latent heat is then efficiently conducted through the tube wall to the erythritol, driving its solid–liquid transition. The physical essence of this process is phase change heat transfer caused by the instantaneous condensation of vapor on the low temperature surface. The tight coupling between HTF vaporization at the source and condensation-induced collapse at the PCM wall creates a dual phase-change synergy. This establishes a highly efficient, heat-pipe-like mechanism that significantly minimizes the system's internal thermal resistance.

Fig. 6(b) illustrates the melting mechanism of PCM (erythritol). This process is fundamentally a physical phenomenon where intermolecular forces progressively dissociate with energy input, and can be divided into the following three stages: ***Stage I (stable solid stage)***: At ambient temperatures, erythritol molecules form an ordered crystal lattice stabilized by van der Waals forces and a robust hydrogen-bonding network. In this regime, molecules exhibit only weak thermal vibrations around their lattice equilibrium positions, and the material maintains stable solid-state characteristics. ***Stage II (lattice loosening stage)***: As heat storage proceeds, heat from HTF condensation conducts through the shell into the PCM. The absorbed thermal energy increases molecular kinetic energy, intensifying thermal motion. As the temperature approaches the PCM melting point (117.0 °C), molecular kinetic energy becomes sufficient to partially overcome the dominant hydrogen bonds. This induces localized lattice defects and structural relaxation, enabling molecules to deviate from their lattice sites and initiate limited range migration. ***Stage III (complete melting stage)***: Upon PCM reaching the melting point, continued heat absorption further elevates molecular kinetic energy until the hydrogen bond network is completely disrupted, causing total crystal collapse. The erythritol transitions fully to the

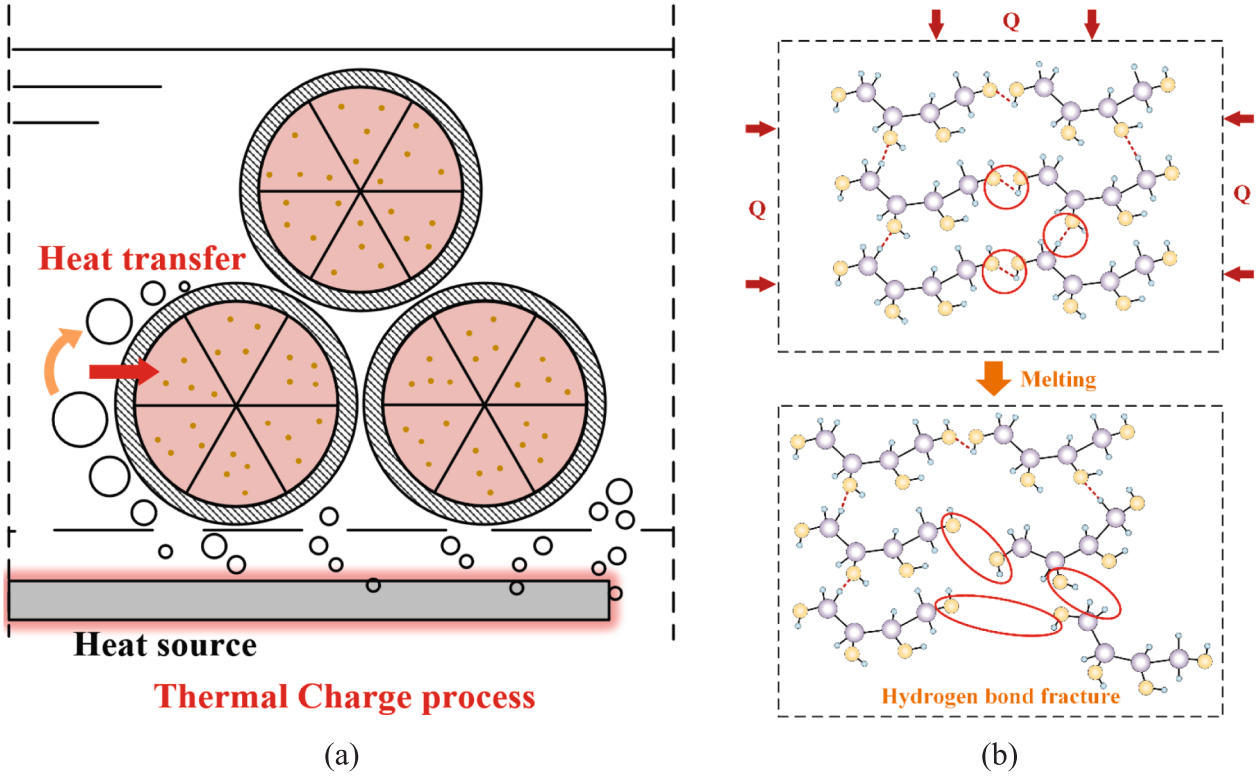

Fig. 6. Melting mechanism of erythritol in the thermal storage device.

liquid phase. The heat absorbed in this stage is primarily used to break intermolecular bonds rather than increase molecular kinetic energy, which maintains a nearly constant system temperature and exemplifies the characteristic isothermal phase change behavior of solid–liquid PCMs.

4.2. Heat release performance

Fig. 7 illustrates the temperature variation trends within the thermal storage device during the heat release process under the water-only condition and different PCM tubes loading quantities conditions (20, 40, and 60 PCM tubes), with a constant cooling water flow rate of 18 L/h through the heat exchange coil. As shown in Fig. 7(a) for the water-only condition, the outlet steam temperature exhibited an initial rise, peaking at 104.5 °C. This initial rapid temperature rise primarily resulted from the release of heat stored in the HTF vapor. After 5.6 min, the output transitioned from superheated steam to steam–water mixture. Thereafter, the outlet temperature gradually decreased, concurrently indicating an increase in water content. The total heat release duration was 23.3 min. When the outlet temperature dropped below 90.0 °C, the condensation system circulation pump stopped operating, halting the heat release process.

As shown in Fig. 7(b), the heat release process could be divided into three stages based on the solidification behavior of the PCM. ***Stage I (rapid HTF heat release stage)***: Upon activation of the circulation pump, coolant enters the heat exchange coil. The coil outlet temperature ascends to 115.2 °C, accompanied by substantial steam discharge. The heat released during this stage primarily came from the sensible and latent heat stored in the vapor HTF. Consequently, the HTF temperature plummets as latent heat is rapidly dissipated, while the PCM temperature decreased slowly. ***Stage II (PCM latent heat release stage)***: When the PCM temperature dropped to approximately 117.8 °C, solidification initiates, releasing latent heat. This latent heat is transferred through a continuous HTF phase-change cycle: the HTF vaporizes by absorbing heat from the PCM and subsequently condenses at the coil to release heat. In this regime, the HTF cooling rate decelerates significantly, the PCM temperature remains quasi-isothermal, and the coil outlet stabilizes at ~ 98.6 °C, establishing a period of stable energy supply. ***Stage III (PCM sensible heat release stage)***: After complete PCM solidification, the system transitions to sensible heat release. With the diminishing influence of latent heat, the temperature decay rates for the HTF, PCM, and coil outlet accelerate. The process terminates when the outlet

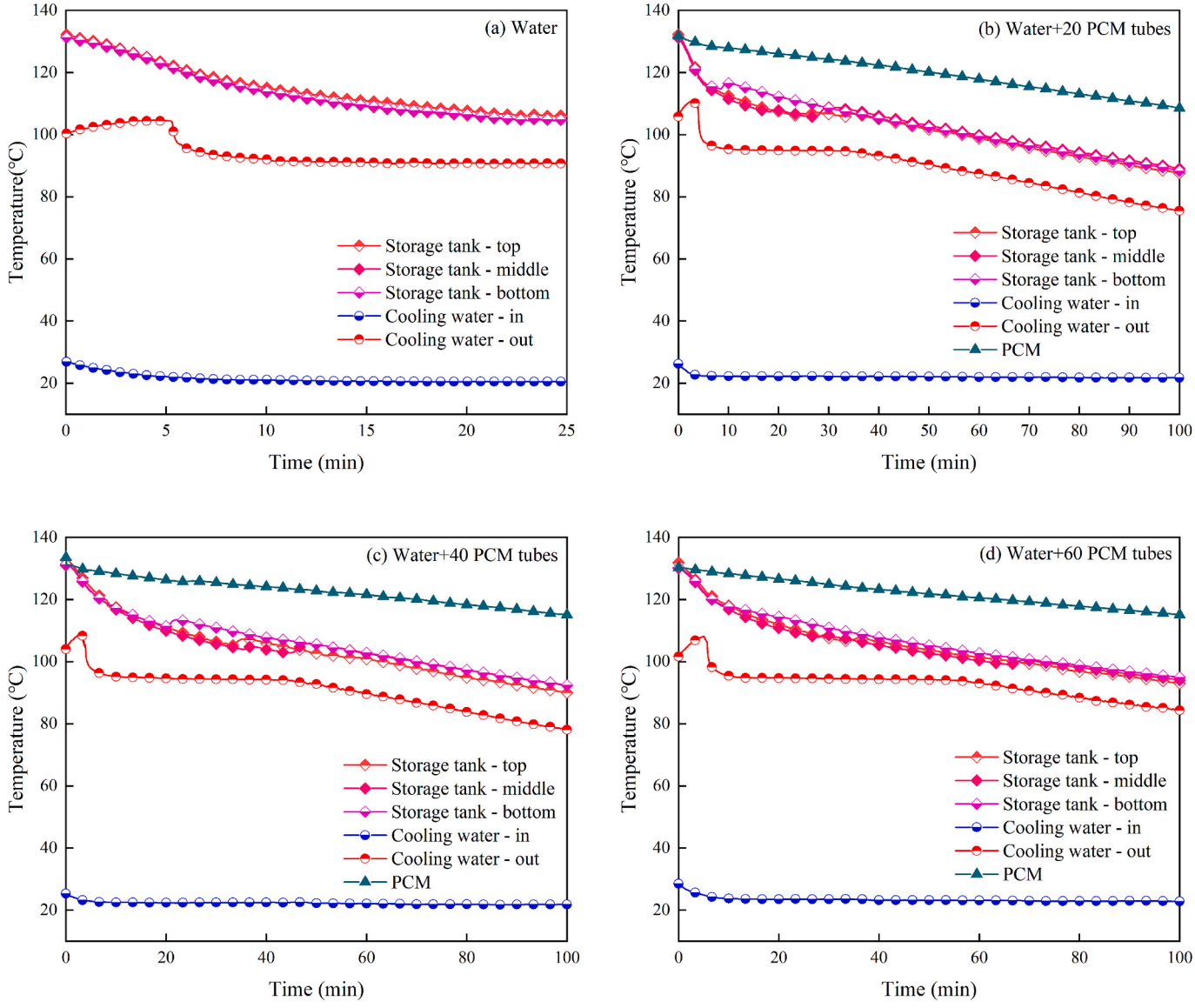

Fig. 7. Temperature during heat release in the TES system coupling solid–liquid and vapor–liquid phase change.

temperature falls below the preset threshold.

Fig. 7(c) and Fig. 7(d) show the temperature variation trends under the conditions of 40 and 60 PCM tubes, respectively. The results indicated that while the temperature trends within the device remained largely consistent across different PCM loading quantities, the system's stable energy supply duration increased significantly with higher PCM quantities. The stable energy supply durations for conditions of 20, 40, and 60 PCM tubes were 53.9 min, 62.2 min, and 77.9 min, respectively. The condition with 60 PCM tubes operated for 54.6 min longer than the water-only condition and 24.0 min longer than the 20 PCM tubes condition. These results confirmed that adding PCM significantly extended energy supply duration under all tested conditions, but the improvement gradually reduced as the number of tubes increased. Additionally, residual working fluid trapped in the coils prior to the circulation initiation caused outlet temperature fluctuations during the initial heat release in all three PCM loading quantities conditions. This phenomenon was attributed to the initial experimental conditions and did not compromise the validity of the comparative analysis.

Fig. 8 shows the heat release power characteristics of the thermal storage device under three different PCM loading quantities conditions. In the initial stage, the substantial amount of heat stored in HTF vapor rapidly heats and vaporizes the working fluid in the heat exchange coil. This allows the system to release heat at a maximum power of 11.1 kW. As the PCM loading quantity increases, the duration for which the system could maintain this peak power increases. Under conditions of 20, 40, and 60 PCM tubes, this duration was 6.2 min, 6.8 min, and 7.7 min, respectively. The average heat release power within 10.0 min was essentially consistent across the three conditions, all approximately 10.8 kW.

As the heat release process progresses, the vaporization rate of the working fluid within the heat exchange coils gradually decreases, leading to a corresponding increase in the water content of the outlet steam-water mixture. Consequently, the system's heat release rate exhibits a gradual downward trend. Considering the average heat release power throughout the entire process, the values for conditions with 20, 40, and 60 PCM tubes were 5.61 kW, 6.44 kW, and 6.68 kW, respectively, showing a slight increase with PCM loading quantity. When the steam–water mixture temperature dropped to approximately 90.0°C, the minimum heat release rates for the three PCM loading quantities conditions were 0.81 kW, 0.95 kW, and 0.96 kW respectively, showing minimal numerical differences. This indicates the system's heat release process had reached its terminal stage.

Fig. 9 compares the total heat released under three different PCM loading quantities conditions with that under the corresponding water-only condition. The results showed that the total heat released under three different PCM loading quantities conditions was significantly higher than that of the corresponding water-only condition. Specifically, for the 20, 40, and 60 PCM tubes conditions, the total heat release energy reached 4.91 kW·h, 6.55 kW·h, and 8.56 kW·h, respectively, whereas the values for the water-only system were 2.36 kW·h, 3.08 kW·h, and 3.83 kW·h under equivalent operating conditions. For the 60 PCM tubes condition, the values were 8.56 kW·h and 3.83 kW·h, respectively. Compared to the water-only system, the addition of PCM increased the total heat released by up to 123.5%. These results clearly demonstrate that PCM loading quantity effectively enhances the system's total heat released, fully showcasing the comprehensive advantages of solid–liquid coupled phase change thermal storage technology in heat release performance.

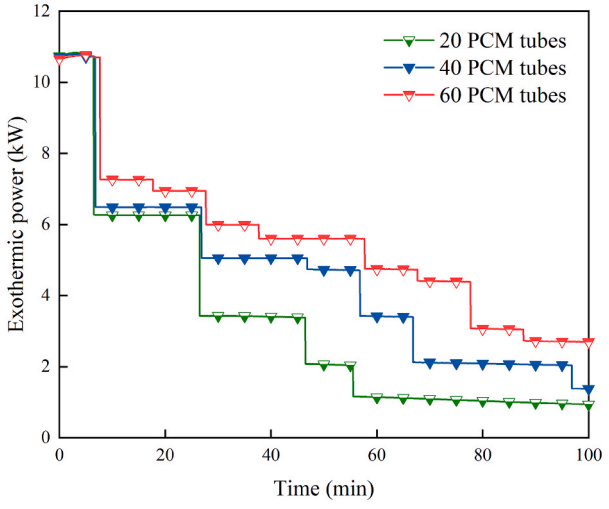

Fig. 8. Heat release power evolution in the TES system coupling solid–liquid and vapor–liquid phase change.

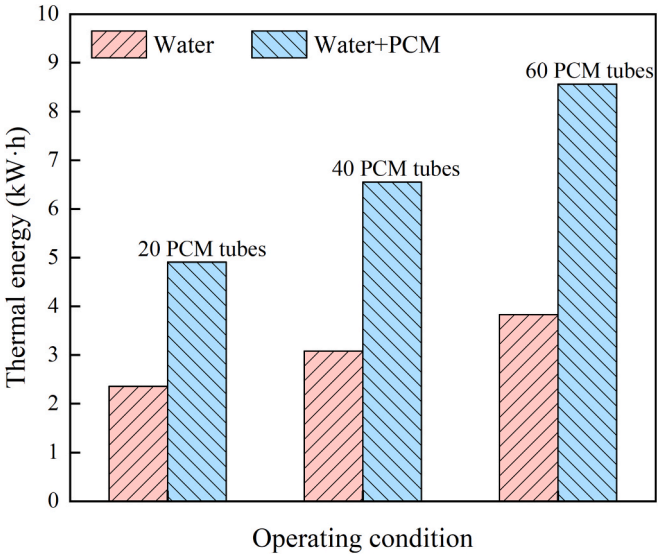

Fig. 9. Comparison of heat released under different conditions.

Fig. 10 illustrates the heat transfer mechanism within the thermal storage device and the PCM solidification mechanism during the heat release process. The heat transfer mechanism during system heat release operation, as depicted in Fig. 10(a), centers on a coupled heat transfer process where latent heat released during PCM solidification drives the phase change cycle of the HTF. Upon entering the condensation system, coolant induces rapid condensation of the vaporized HTF on the outer coil surface, transferring both latent and sensible heat to the coolant. This condensation causes a gradual decline in internal system pressure, thereby lowering the HTF saturation temperature. Concurrently, the heat liberated from PCM solidification acts to sustain the HTF temperature near this pressure-dependent saturation point. The condensed liquid HTF drops into the PCM region, undergoes flash vaporization upon absorbing heat released by the PCM, and the vapor rises back to the outer surface of the coil where it recondenses. This establishes a continuous HTF flash vaporization–condensation phase change cycle. This cycle serves as an efficient heat transfer pathway for PCM's heat release, tightly coupling the PCM, HTF, and condensation system. It is essential to embed the HTF's phase change flow process within the PCM's heat release process. It significantly mitigates overall thermal resistance, facilitating rapid and stable energy delivery.

The solidification mechanism of the PCM (erythritol) is illustrated in Fig. 10(b). This process is fundamentally a physical phenomenon involving the reduction of molecular kinetic energy and the reconstruction of the crystal lattice. The process evolves through three distinct stages: ***Stage I (liquid cooling)***: During the initial discharging phase, liquid erythritol releases sensible heat, causing a gradual temperature decline. As the average molecular kinetic energy diminishes, the intensity and frequency of thermal motion decrease, yet the molecules

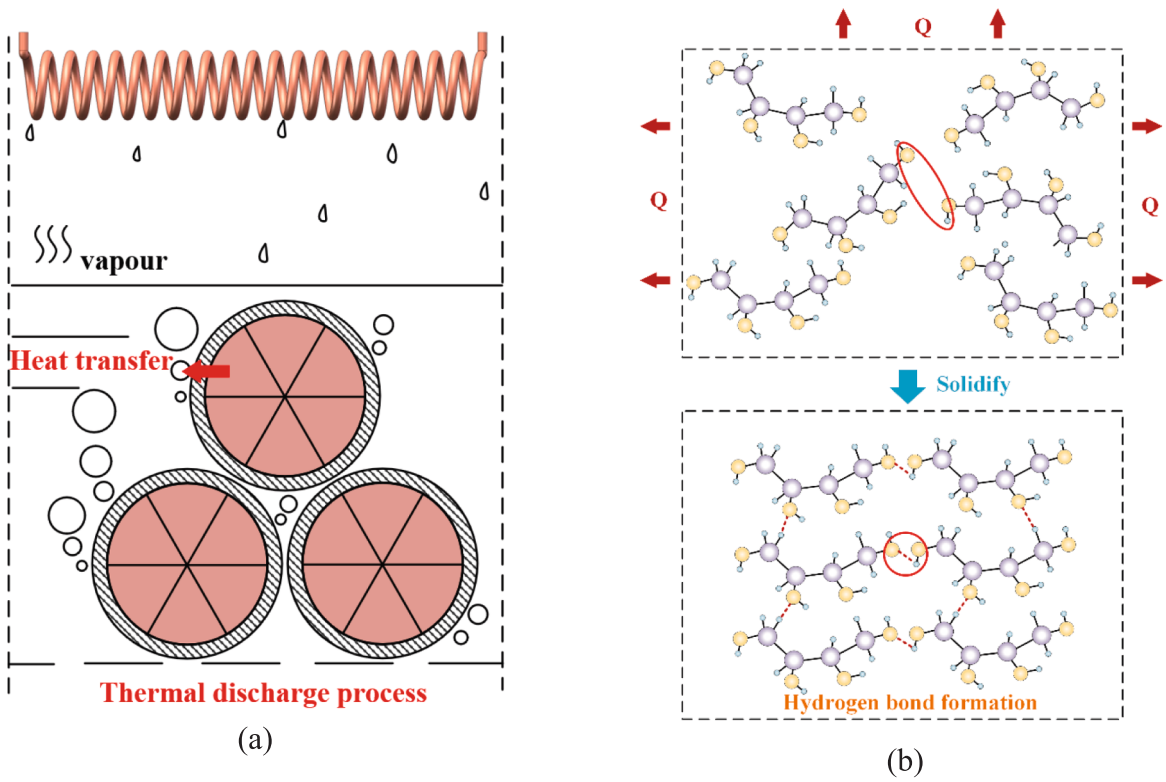

Fig. 10. Solidification mechanism of erythritol in the thermal storage device.

remain in a disordered, mobile state. ***Stage II (molecular aggregation stage)***: As the process of heat release progresses, the amplitude of thermal motion reduces significantly, and intermolecular distances contract. At this point, intermolecular forces—primarily van der Waals interactions and hydrogen bonding—begin to dominate. These forces drive the randomly moving molecules to aggregate into ordered clusters, establishing the nuclei necessary for lattice formation. ***Stage III (lattice reconstruction)***: With continued heat extraction, molecular kinetic energy becomes insufficient to overcome the attractive intermolecular forces. Molecules progressively stabilize and rearrange at lattice sites, gradually forming an ordered crystal structure, ultimately completing the liquid to solid transition.

4.3. Thermal efficiency analysis

Fig. 11 presents the system thermal efficiency as a function of the PCM filling ratio. The results reveal system thermal efficiency was positively correlated with PCM filling ratio, but the increase in efficiency gradually diminished as the filling ratio increased. At PCM filling ratios of 14.3% (20 tubes, 38.4 kg), 28.6% (40 tubes, 76.8 kg), and 42.9% (60 tubes, 115.2 kg), the system achieved thermal efficiencies of 0.58, 0.67, and 0.73, respectively. As the PCM filling ratio increased to 92.8%, the system thermal efficiency reached a peak of approximately 0.84. Further increases in PCM filling ratio caused the efficiency to stabilize. This phenomenon primarily stemmed from the influence of the PCM filling ratio on the energy distribution structure. As the PCM filling ratio increased, a larger proportion of the input energy was stored in the PCM, while the relative share of fixed losses such as heat dissipation to the surroundings and inevitable heat losses during heat transfer decreased, thereby enhancing system efficiency. Once the PCM filling ratio exceeds a critical threshold, the proportion of fixed losses dropped to a low level, limiting further efficiency gains and leading to a gradual stabilization phase.

The variation in system thermal efficiency with PCM filling ratio is governed by the shifting proportions of three distinct energy loss

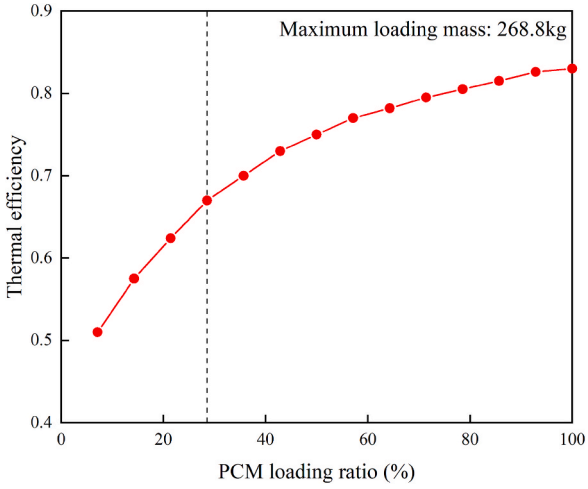

Fig. 11. Thermal efficiency of the TES system coupling solid–liquid and vapor–liquid phase change under different PCM filling ratios.

mechanisms relative to the total input energy. ***Heat loss from the storage tank***: Despite the insulation applied to the outer walls of the thermal storage device, heat was still dissipated to the environment through conduction and convection during heat storage/release processes. At low PCM filling ratios, the system's limited total storage capacity results in a disproportionately high fraction of energy lost to dissipation, thereby depressing thermal efficiency. As the filling ratio increases, the substantial rise in total stored energy dilutes the relative impact of these fixed dissipative losses, mitigating their negative effect on overall efficiency. ***Heat transfer loss***: Energy transfer from the electric heating tubes to the PCM via HTF involves multiple heat exchange stages, each presenting thermal resistance and heat dissipation. Increased PCM filling enhances thermal buffering capacity, reducing HTF circulation

frequency and minimizing heat loss during transfer, thereby decreasing the proportion of losses in this segment. ***Heat loss from PCM properties***: The erythritol used exhibits supercooling during the phase change process, which not only delays the heat release process but also increases the amount of heat dissipated to the environment, thereby adversely affecting the system's thermal efficiency. The present study focuses primarily on the overall thermal performance of the thermal storage system and does not specifically investigate the impact of PCM supercooling on system thermal performance in depth.

Against the backdrop of deepening electricity market reforms and policies promoting high-penetration renewable integration, high-efficiency thermal energy storage (TES) systems are poised to deliver significant economic value. On one hand, central and local governments have lowered investment barriers through incentives such as ancillary service compensation and subsidies for co-located storage systems. On the other hand, many regions in China have adopted deep peak-valley time-of-use pricing, with renewable-rich areas occasionally experiencing extended periods of negative electricity prices—effectively enabling near-zero-cost charging. Under these market and policy conditions, the TES system proposed in this study not only enhances operational flexibility and dispatchability but also allows cost-effective—or even free—thermal charging during off-peak or negative-price hours, followed by heat discharge during peak periods to capture revenue, thereby demonstrating strong economic viability and commercial potential.

5. Conclusion

A TES method that couples vapor–liquid and solid–liquid phase change processes was proposed. A series of experiments was conducted using erythritol as the PCM and deionized water as the HTF to investigate the system's thermal performance at different PCM filling ratios. The key findings of the study are summarized below:

(1) When the system operated in heat storage mode, the total duration for heat storage increases with the amount of PCM loaded, but this increase rate gradually decelerates. Under conditions with 20, 40, and 60 PCM tubes, the total duration of the heat storage process was 46.3 min, 59.6 min, and 71.5 min, respectively. The PCM melting durations were 8.1 min, 17.1 min, and 24.6 min, with PCM temperatures stabilizing between 116.9 °C and 118.5 °C during the heat storage process. Increasing the PCM filling ratio led to greater temperature response delay at the bottom of the device, with the maximum temperature difference reaching 47.9 °C between the bottom and the top region. When storing the same amount of energy, erythritol's volumetric energy density was significantly higher than that of water.

(2) When the system operated in heat release mode, the duration of the heat release process under water-only conditions was 23.3 min, while the condition with 60 PCM tubes achieved the longest sustained energy supply time of 77.9 min. In terms of average heat release power, the conditions with 20, 40, and 60 PCM tubes delivered 5.61 kW, 6.44 kW, and 6.68 kW, respectively. Compared to the water-only condition, the addition of PCM significantly extended the heat release process duration and increased the total heat release capacity by 123.5%. As the heat release progressed, the power gradually decreased due to the rising water content in the steam-water mixture. Overall, the power decline trend was consistent across all conditions, indicating the system's stable heat release characteristics. The addition of PCM effectively extended the heat release duration and enhanced the heat release power, confirming its role in enhancing the system's heat release capability.

(3) System thermal efficiency showed a positive correlation with PCM filling ratio. When the PCM loading quantity corresponded to 20, 40, and 60 tubes (equivalent to filling ratio of 14.3%, 28.6%, and 42.9%), the system energy efficiencies were 0.58, 0.67, and 0.73, respectively. When the PCM filling ratio reached 92.8%, efficiency reached 0.84 and then stabilized, with the rate of increase gradually decreasing as the filling ratio increased. System heat losses primarily originated from three sources: storage tank heat dissipation, heat transfer losses, and PCM supercooling. As the PCM filling ratio increased, the proportion of these losses in the total input energy decreased, leading to efficiency improvement. Once the PCM filling ratio exceeded a critical threshold, the loss proportion remained at a low level, limiting further efficiency gains and thus restricting potential improvements in thermal efficiency.

CRediT authorship contribution statement

Chaofan Qu: Writing – review & editing, Writing – original draft, Validation, Methodology, Investigation, Data curation, Conceptualization. **Zhaoxu Zhu:** Investigation, Data curation. **Yiming Xie:** Investigation, Data curation. **Xianbing Ji:** Writing – review & editing, Writing – original draft, Project administration, Methodology, Investigation, Conceptualization. **Jinliang Xu:** Writing – review & editing, Methodology, Conceptualization. **Zheng Miao:** Writing – review & editing, Methodology.

Declaration of competing interest

The authors declare that they have no known competing financial interests or personal relationships that could have appeared to influence the work reported in this paper.

Acknowledgment

This research was supported by the National Natural Science Foundation of China (Nos. 52176154, 52476007).

Data availability

Data will be made available on request.

References

[1] International Renewable Energy Agency. Thermal energy storage: technology brief. Abu Dhabi: International Renewable Energy Agency; 2020.
[2] Farid MM, Khudhair AM, Razack SAK, Al-Hallaj S. A review on phase change energy storage: Materials and applications. Energy Convers Manag 2004;45:1597–615. https://doi.org/10.1016/j.enconman.2003.09.015.
[3] Peng G, Dou G, Hu Y, Sun Y, Chen Z. Phase Change Material (PCM) Microcapsules for Thermal Energy Storage. Adv. Polym. Technol. 2020:9490873. https://doi.org/10.1155/2020/9490873.
[4] Gunasekara SN, Pan R, Chiu JN, Martin V. Polyols as phase change materials for thermal energy storage: properties and applications. Appl Energy 2016;178:142–57. https://doi.org/10.1016/j.apenergy.2015.03.064.
[5] Paul J, Kadirgama K, Samykano M, Pandey AK, Tyagi VV. A comprehensive review on thermophysical properties and solar thermal applications of organic nano composite phase change materials. J Energy Storage 2022;45:103415. https://doi.org/10.1016/j.est.2021.103415.
[6] Zhang Q, Ma F, Liu L, Tan W, Jing M, Wang L, et al. Recent advances in nano-enhanced phase change materials. J Mater Sci 2024;59:5247–67. https://doi.org/10.1007/s10853-023-08830-8.
[7] Paul D, Biswas N, Bhattacharyya S, Alshehery S, Togun H, Alreshidi MA, et al. A comprehensive review on composite phase change materials for sustainable thermal energy solutions: Advances and barriers. Sustain Mater Technol 2025;45:e01578. https://doi.org/10.1016/j.susmat.2025.e01578.
[8] Hu R. Fundamental experimental study on a gravity heat pipe medium-temperature phase change heat storage device. Shanghai Jiao Tong University; 2014. Master's thesis.
[9] Mao S, Liu Y, Wu X, Zhang L, Chen J, Zhou T. Thermal energy storage performance, application and challenge of phase change materials: a review. Energy Storage Sav 2025. https://doi.org/10.1016/j.enss.2025.03.001.
[10] He S, Wang W, Wei L, Ding J. Heat transfer enhancement and melting behavior of phase change material in a direct-contact thermal energy storage container. J Energy Storage 2020;31:101665. https://doi.org/10.1016/j.est.2020.101665.

[11] He S, Ling Z, Fang X, Zhang Z. Experimental study on an improved direct-contact thermal energy storage container. J Energy Storage 2024;102:114201. https://doi.org/10.1016/j.est.2024.114201.
[12] Thon H, Simonsen G, Leinan PR. Controlled operation of a direct contact thermal energy storage device. Chem Eng Sci 2025;308:121385. https://doi.org/10.1016/j.ces.2025.121385.
[13] Kang Z, Zhou W, Qiu K, Wang C, Qin Z, Zhang B, et al. Numerical simulation of an indirect contact mobilized thermal energy storage container with different tube bundle layout and fin structure. Sustainability 2023;15:5511. https://doi.org/10.3390/su15065511.
[14] Al-Mudhafar AHN, Nowakowski AF, Nicolleau FCGA. Performance enhancement of PCM latent heat thermal energy storage system utilizing a modified webbed tube heat exchanger. Energy Rep 2020;6:76–85. https://doi.org/10.1016/j.egyr.2020.02.030.
[15] Zhao C, Jia C, Xu L, Zhang F, Qi D, Song B, et al. Heat transfer enhancement of PCM in the triple-pipe helical-coiled latent heat thermal energy storage unit and complete melting time correlation. Renew Energy 2024;236:121528. https://doi.org/10.1016/j.renene.2024.121528.
[16] Maldonado JM, Verez D, Gracia AD, Cabeza LF. Comparative study between heat pipe and shell-and-tube thermal energy storage. Appl Therm Eng 2021;192:116974. https://doi.org/10.1016/j.applthermaleng.2021.116974.
[17] Saraswat A, Bhattacharjee R, Verma A, Das MK, Khandekar S. Investigation of diffusional transport of heat and its enhancement in phase-change thermal energy storage systems. Appl Therm Eng 2017;111:1611–21. https://doi.org/10.1016/j.applthermaleng.2016.06.178.
[18] Zhao J, Dai Y, Wang Z, Liu Y, Xu W, Mao Y, et al. Study on the thermal performance of thermal energy storage and heating module based on a novel embedded heat pipe. J Energy Storage 2022;52:104743. https://doi.org/10.1016/j.est.2022.104743.
[19] Saffarian MR, Fazelpour F, Sham M. Numerical study of shell and tube heat exchanger with different cross-section tubes and combined tubes. Int J Energy Environ Eng 2019;10:33–46. https://doi.org/10.1007/s40095-019-0297-9.
[20] Mahato SK, Rana SC, Barman RN. Study of heat transfer enhancement through the non-circular ducts using three dimensional numerical investigations and their comparisons. IOP Conf Ser: Mater Sci Eng 2021;1128:012037. https://doi.org/10.1088/1757-899X/1128/1/012037.
[21] Kurşun B, Balta M. Evaluation of the different inner and outer channel geometry combinations for optimum melting and solidification performance in double pipe energy storage with phase change material: A numerical study. Energy Storage 2023;65:107250. https://doi.org/10.1016/j.est.2023.107250.
[22] Yu J, Zhang G, Zhang Z, Liu X, Rao Z. Numerical study on novel fin configurations for enhancing thermal performance of latent heat thermal energy storage systems. Appl Therm Eng 2025;278:127381. https://doi.org/10.1016/j.applthermaleng.2025.127381.
[23] Tang S, Song Y, Liu P, Wu X, Li X, Xu Y. Experimental study on melting performance and uniformity of thermal energy storage systems with discontinuous fins. Appl Therm Eng 2025;278:127429. https://doi.org/10.1016/j.applthermaleng.2025.127429.
[24] Tang S, Song Y, Liu P, Wu X, Li X, Xu Y. Experimental study on improving the rapid response performance of modular latent thermal energy storage by topological fins. Appl Therm Eng 2025;277:126976. https://doi.org/10.1016/j.applthermaleng.2025.126976.
[25] Peiró G, Gasia J, Miró L, Cabeza LF. Experimental evaluation at pilot plant scale of multiple PCMs (cascaded) vs. Single PCM configuration for thermal energy storage. Renew Energy 2015;83:729–36. https://doi.org/10.1016/j.renene.2015.05.029.
[26] B.M. Suyitno, Ismail, R.A. Rahman, Improving the performance of a small-scale cascade latent heat storage system by using gradual melting temperature storage tank, Case Stud. Therm. Eng. 45 (2023) 103034, https://doi.org/10.1016/j.csite.2023.103034.
[27] Rudra Murthy BV, Nidhul K, Gumtapure V. Performance evaluation of novel tapered shell and tube cascaded latent heat thermal energy storage. Sol Energy 214 2021:377–92. https://doi.org/10.1016/j.solener.2020.11.069.
[28] Elsanusi OS, Nsofor EC. Melting of multiple PCMs with different arrangements inside a heat exchanger for energy storage. Appl Therm Eng 2021;185:116046. https://doi.org/10.1016/j.applthermaleng.2020.116046.
[29] Pal S, Bhanja D, Misra RD. Simulation on PCM melting improvement with triple-finned horizontal shell-tube latent-heat thermal energy storage unit: Effect of fin size and distribution. J Energy Storage 2025;134:118195. https://doi.org/10.1016/j.est.2025.118195.
[30] Zheng W, Yang S, Li W, Luo M, Song C, Zhang Y. Experimental study on thermal performance of phase change heat storage device with rectangular shell structure. Appl Therm Eng 2022;214:118897. https://doi.org/10.1016/j.applthermaleng.2022.118897.